ISSN 0036-0236, Russian Journal of Inorganic Chemistry, 2016, Vol. 61, No. 3, pp. 265–272. © Pleiades Publishing, Ltd., 2016.
Original Russian Text © A.V. Severin, D.A. Pankratov, 2016, published in Zhurnal Neorganicheskoi Khimii, 2016, Vol. 61, No. 3, pp. 279–287.

SYNTHESIS AND PROPERTIES OF INORGANIC COMPOUNDS

Synthesis of Nanohydroxyapatite in the Presence of Iron(III) Ions

A. V. Severin and D. A. Pankratov

Moscow State University, Moscow, 119991 Russia

e-mail: severin@radio.chem.msu.ru

Received April 15, 2015

Abstract—The effect of small amounts of iron(III) ions on the morphology, phase composition, and structure of the products of the hydroxyapatite (HAP) synthesis has been studied by electron microscopy, X-ray powder diffraction, and Mossbauer spectroscopy methods. It has been demonstrated that the introduction of dopant iron(III) ions into the reaction mixture at different stages of HAP formation makes it possible to control crystal growth, morphology, and phase composition. The iron ions are not incorporated into the HAP crystal structure; rather, they form their proper nanophase, as well as adsorption clusters on the HAP surface.

DOI: 10.1134/S0036023616030190

Hydroxyapatite (HAP)—the inorganic matrix of bone tissue—is among the most popular biomaterials in medical and biochemical practice (bone surgery, stomatology, creation of implants or coatings for metal implants in orthopedics, etc. [1, 2]). The presence of transition-metal impurities in HAP (when they are substituted for Ca^{2+} ions or when they form stable adsorption complexes on the HAP crystal surface) can noticeably change its physicochemical properties, such as solubility, thermal stability, biochemical activity, magnetic properties, and mechanical durability. Some biologically active metals (for example, zinc, magnesium, iron, or manganese) present as impurities in HAP can stimulate bone tissue formation and differentiation since they are natural components of bone tissue [3]. Nevertheless, a specific role of many metals in rigid tissue and their potential medical application is still unclear. At the same time, composite materials containing HAP nanoparticles with transition-metal (Cu, Co, Fe, etc.) compounds as nanocatalysts (for example, for glycerol conversion [4] or formaldehyde oxidation [5]) have found increasing application in recent years. Substitution of transition metal for calcium ions in HAP can lead to the formation of colored products, which can be used as safe pigment dyes [6].

Among HAP composites with metal compounds, iron holds a special position. First, apatite-like structures in which iron ions can be substituted for calcium ions can function as precursors of de novo bone tissue and enhance the proliferative activity of osteoblasts (cells that make bone) [7]. Second, numerous recent efforts have focused on composites of HAP crystals with magnetic iron-containing particles of different nature [8–12]. Heightened interest in such compounds is due to the development and improvement of methods of magnetic therapy for cancer, in particular, for different types of bone cancer [8, 9]. In this case, HAP particles serve as both the carriers of the therapeutic magnetic iron and the building material for healthy bone tissue. Third, in addition to widespread medical applications, HAP–Fe composites as specific carriers of different metal-containing nanocatalysts enhancing their activity have been reported [10].

Available literature data demonstrate that HAP composites with iron(III) ions are mainly of three types: composites where iron(III) ions are incorporated in the HAP crystal structure through substitution for one of the calcium ions in it [10]; composites in which these ions are adsorbed (as ions or nanoclusters) on the surface of HAP nanocrystals [11]; composites in which iron(III) compounds form their proper nanophase [12]. Each of these forms is synthesized by a special procedure with a wide variation of synthesis and post-synthesis treatment conditions [10–12]. In the present work, control of the moment of introduction of iron(III) compounds into the system of reagents allowed us to produce all three forms of composites in a single experiment. As distinct from the earlier experiments, we introduced a maximal iron amount possible under given conditions (but not more than 7.5% of the HAP weight).

EXPERIMENTAL

HAP was synthesized as described in [13]. To do this, an aqueous suspension of calcium oxide was mixed in a special reactor with a 30% orthophosphoric acid solution in the 10 : 6 ratio, which corresponded to the stoichiometry of the target compound. The reagent concentrations were selected to give a 5% suspension of the product. The orthophosphoric acid solution was added to the reaction mixture at a controlled rate, and the course of formation of nanohy-

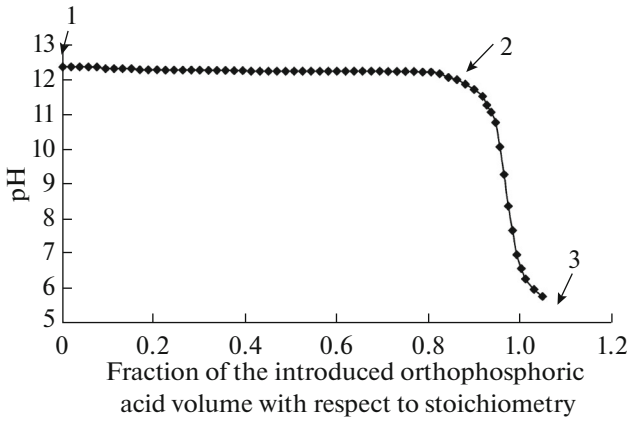

Fig. 1. Change in pH of the reaction mixture in the course of HAP synthesis (the moments of introduction of iron-containing solutions into the reaction mixture are specified).

droxyapatite (according to [13], exclusively HAP is formed under the given experimental conditions) was monitored by observing the change in pH of solutions (an MV88 pH meter, accuracy 0.01 pH) (Fig. 1). It is believed that the reaction of the reagents is completed after adding the stoichiometric amount of orthophosphoric acid or after pH 6–7 was achieved according to calcium phosphate solubility diagrams [14].

Here, the stage of introduction of an iron(III) sulfate solution into the reaction mixture at different moments of HAP formation was added to the procedure described above (Fig. 1). An iron-containing solution was prepared from $Fe_2(SO_4)_3 \cdot 9H_2O$ (pure grade). Its concentration was taken such that, after the addition of 20 mL of this solution to the solution of the reagents, the resulting HAP contained 0.015 g of iron(III) per 0.2 g HAP (i.e., approximately 7.5 wt %). The iron(III) content in the initial solution was monitored by complexometric titration (EDTA, acetate buffer solution, pH 2–3, fluorexon as an indicator) and spectrophotometry (*o*-phenanthroline, hydroxylamine buffer) [15].

We studied the products that formed after the introduction of an iron(III) solution at three different stages if the HAP synthesis (Fig. 1):

(1) before the introduction of orthophosphoric acid into an aqueous suspension of calcium oxide (hereinafter, samples **1x**);

(2) at the point of the onset of the sharp decrease in pH of the solution (Fig. 1; hereinafter, samples **2x**);

(3) after the completion of HAP formation (hereinafter, samples **3x**).

After the basic synthesis was completed, the reaction mixture was stirred for 2 h; then, the resulting suspension was centrifuged, and the solid phase was separated. The precipitate was dried to constant weight at 80°C, ground in a porcelain mortar, and kept in glass bottles (hereinafter, sample **Na**). Then, a portion of the dry powders was annealed in a muffle furnace in air at 500°C for 6 h (hereinafter, sample **Nc**).

Thus, we prepared six samples (denoted as **Nx**) that differ in the moment of introduction of iron ions into the reaction mixture (before, during, and after the synthesis of HAP) and in conditions of thermal treatment of HAP crystallites (dried at 80°C and annealed at 500°C) (Table 1).

The iron content in solid samples after synthesis was monitored by spectrophotometry (*o*-phenanthroline, hydroxylamine buffer solution) after dissolving weighed portions in concentrated nitric acid. For example, for samples of series **Na**, the iron content was 7.0 ± 1.0 wt %.

The morphology of nanocrystals was studied by transmission electron microscopy (a Jeol JEM-1011B transmission electron microscope, resolution 0.3 nm). Some samples were additionally studied by high-resolution transmission electron microscopy (a Jeol JEM-2100F transmission electron microscope). Materials for TEM were sampled from aqueous suspensions before phase separation. Drops of the suspension diluted with distilled water in the 30 : 1 ratio were applied to a copper grid with a formvar film, and dried in air.

The phase composition of the dry HAP samples was monitored by means of X-ray powder diffraction (XRD). X-ray powder diffraction patterns were recorded on an automated DRON-3 diffractometer (CuK_α radiation, 0.1542 nm, graphite monochromator in the diffracted beam, stepwise scanning at a step of 0.1°–0.05°) in the Bragg–Brentano geometry operated with the EXPRESS software. The counting time was 3–5 s per point. The X-ray powder diffraction patterns were processed with the PHAN and PHAN% programs [16].

Adsorption Mössbauer spectra were recorded on an MS1101E express Mössbauer spectrometer (MosTec company, Rostov-on-Don). The Mössbauer source was ^{57}Co in a rhodium metal matrix with an activity up to 15 mCi (RITVERC GmbH, St. Petersburg). The isomer shifts were referenced to α-Fe. The spectra of crystalline HAP samples were recorded at room and liquid-nitrogen temperatures. The spectra were fitted with a few symmetric doublets with the use of the Univem MS 4.02 software.

RESULTS AND DISCUSSION

We synthesized six different HAP–Fe composites, and their color changed from light beige to dark brown depending on synthesis conditions. The major differences between these samples are in the conditions of introduction of iron(III) ions in the reaction mixture in the course of HAP synthesis and in conditions of post-synthesis treatment of the products (Table 1). The moment of introduction of dopant iron(III) ions into the reaction mixture was determined by the

Table 1. HAP synthesis conditions with different moments of introduction of 20 mL of a Fe(III) solution

Sample	Treatment temperature, °C	Acid feeding rate, mL/min	H_3PO_4 (30%) volume, mL	pH range in the course of synthesis	Note
1a	25.6	0.90	15.10	13.2–7.0	Iron(III) solution was introduced before the addition of the acid
2a	24.3	0.67	16.85	13.9–5.8	Iron(III) solution was introduced at the moment of the sharp decrease in pH
3a	23.0	0.75	16.80	13.3–7.0	Iron(III) solution was introduced after the completion of HAP synthesis
1c	500	Analogously to **1a**			Heating for 6 h
2c	500	Analogously to **2a**			″
3c	500	Analogously to **3a**			″

change in its pH during the reaction of the calcium hydroxide suspension and an orthophosphoric acid solution. It can be a priori assumed that the introduction of iron sulfate into the initial calcium hydroxide suspension (1x) should lead to the formation of iron(III) hydroxide particles [17], which could later act as HAP crystallization centers. At the same time, the introduction of iron sulfate at the final stage of HAP synthesis (**3x**) could evidently lead to the formation of iron phosphate particles [18, 19] on the surface of the synthesized HAP. The development of the system when iron(III) sulfate is added at the moment of HAP phase formation (**2x**) is of most interest. In this case, both the cocrystallization of iron and calcium phosphates and the formation of separate iron-containing phases are possible, which can has an effect on the HAP particle growth. The isolation of the precipitate immediately after its crystallization (**Na**) should evidently lead to a poorly structured material. Annealing the materials at 500°C (**Nc**) was aimed to intensify phase recrystallization to thermodynamically more stable forms, but it was undoubtedly accompanied by the change in the phase composition because of water removal from the samples [20].

XRD data demonstrate that the major crystalline phase contained in all **Na** samples is HAP (Fig. 2). In particular, the XRD patterns of samples **2a** and **3a** are almost identical and show all basic reflections corresponding to hexagonal HAP [21, 22]. In addition, the XRD patterns of all samples show a rather strong reflection at 29.8° (2.998 Å) corresponding to calcium sulfate hemihydrate [23], which is evidently formed from calcium sulfate dehydrate [24] in the course of drying at 80°C [25]. The presence of the basanite impurity in the sample is presumably a reason of the considerable broadening HAP reflections in the XRD patterns because of their superposition. For sample **1a**, this reflection is considerably weaker, but the reflection at 23° (3.867 Å) corresponding to the reflection from the 111 plane of HAP becomes more clearly pronounced. It is evident that calcium sulfate forming upon the introduction of iron sulfate at the early stage of synthesis has a lower possibility to recrystallize in the course of synthesis to give bulky crystallites; i.e.,

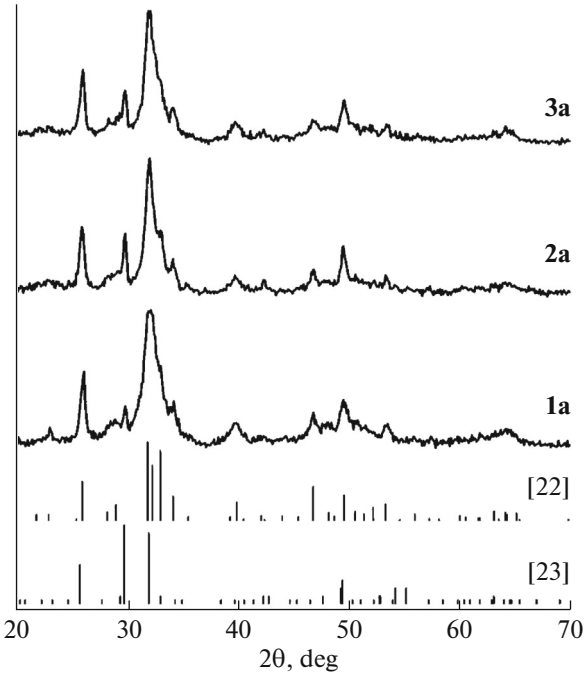

Fig. 2. XRD diagrams for $CaSO_4 \cdot 0.5H_2O$ [23] and $Ca_5(PO_4)_3(OH)$ [22] and experimental XRD patterns for samples **1a**, **2a**, and **3a**.

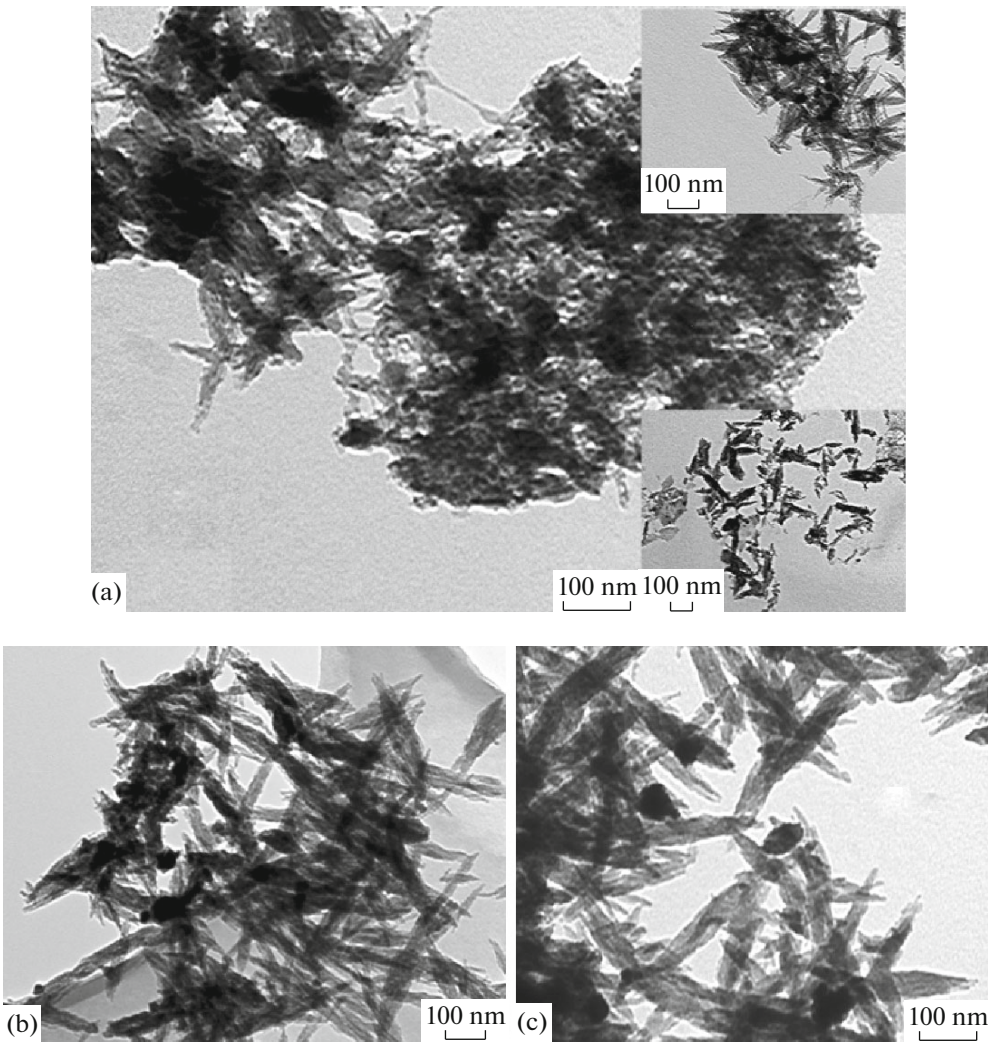

Fig. 3. Morphology of HAP–Fe nanocrystals obtained after introducing iron(III) ions at different stages of HAP synthesis: (a) **1a**, (b) **2a**, and (c) **3a**.

HAP is capsulated. For all the samples, diffraction lines can be assigned to none of iron-containing phases, including iron phosphate. It is likely that the forming iron(III) compounds are mainly in the nanosized and/or X-ray amorphous state.

The XRD patterns of the samples heat treated at 500°C differ from the initial sample only by narrower reflections of the HAP phase and a considerably weaker reflection of basanite at 29.8° 2θ (especially for samples **2c** and **3c**) because of its dehydration to anhydrite [26]. The relatively smaller change in the intensity of the corresponding reflection for sample **1c** is indirect evidence of capsulation of calcium sulfate of HAP. It is evident that they could be HAP crystallization centers in sample **1x**.

The morphology of the resulting nanosized HAP crystallites was studied by electron microscopy (Figs. 3a–3c). It follows from these data that samples **2a** and **3a** are morphologically very similar to each other (Figs. 3b and 3c), which is consistent with XRD data. The length (L) and width (H) distribution functions of nanocrystals calculated from the electron microscopy data are similar to each other (Fig. 4, curves *1* and *2*), although nanocrystals in samples **2a** are somewhat smaller. This is presumably evidence that iron(III) ions hinder the growth and aggregation of HAP nanoparticles through blocking of the crystal surface in adsorption [9, 27].

For sample **1a**, the effect of the iron(III) sulfate impurity on the HAP morphology is even more pronounced. According to TEM data, this sample is morphologically inhomogeneous (Fig. 3a) as distinct from the above samples; this prevents us to construct a common distribution function. This morphological inhomogeneity can be caused by the presence of impurity crystals (calcium sulfate, on the one hand, and iron(III) hydroxide itself, on the other) acting as aggregation and growth centers of the major phase. In

addition, there is observed a fractal shape of aggregates in the sample, which can be formed by amorphized HAP particles produced because of the crystallization-hindering action of iron(III) ions.

The above assumptions that, in nearly all the samples, iron can form, in addition to the other phases, its own nanophase and iron-containing clusters (or their aggregates) adsorbed on the HAP surface are supported by high-resolution TEM and energy-dispersive electron probe microanalysis data (Fig. 5). It has been demonstrated that separate nanoparticles and spots on the HAP nanocrystals are due to precisely iron compounds. Formation of similar clusters of iron compounds on the surface of HAP nanoparticles has been already described [28].

The heat treatment of samples at 500°C leads to the expected change in particle morphology characteristic of HAP [29]. After this treatment, particles acquire a more isometric shape and become optically denser (their thickness increases), and their size changes with respect to the initial one according to distribution functions (Fig. 4, curves *3* and *4*).

The Mössbauer spectra of the samples at various temperatures are well-resolved doublets, symmetric or slightly asymmetric depending on the sample (Fig. 6). All experimentally observed doublets are fitted with two superimposed symmetric doublets with close isomer shift values (Table 2) corresponding to octahedral iron(III) compounds [30], but with rather different quadrupole splitting values and line widths (Table 2).

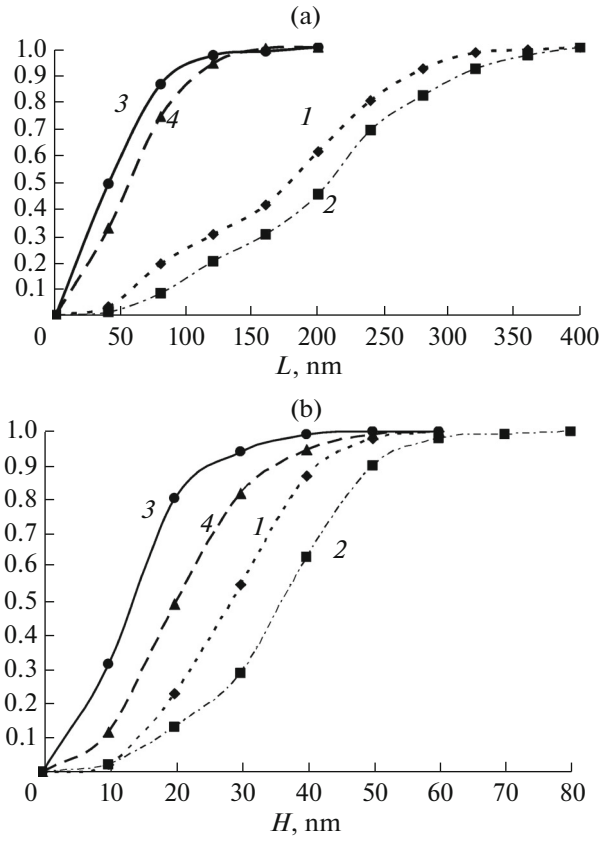

Fig. 4. (a) Length *L* and (b) width *H* distribution functions of nanocrystals of samples (*1*) **2a**, (*2*) **3a**, (*3*) **2c**, and (*4*) **3c**.

Table 2. Mössbauer parameters of the samples*

Sample	Temperature	δ		Δ		Γ_{exp}		*I*		*S*	
		1	2	1	2	1	2	1	2	1	2
	K	mm/s						%			
1a	79	0.47	0.46	0.64	1.04	0.38	0.61	2.84	4.80	27	73
	300	0.37	0.37	0.64	1.03	0.39	0.60	2.38	3.50	31	69
2a	79	0.52	0.50	0.58	1.01	0.37	0.58	4.50	6.01	33	67
	300	0.41	0.39	0.57	0.96	0.37	0.58	2.90	4.31	30	70
3a	79	0.47	0.45	0.55	0.93	0.33	0.56	2.15	4.99	20	80
	300	0.41	0.39	0.55	0.91	0.33	0.56	1.65	4.07	20	80
1c	79	0.48	0.46	0.78	1.32	0.49	0.76	3.59	4.39	35	65
	300	0.37	0.35	0.78	1.29	0.46	0.74	2.73	3.35	34	66
2c	79	0.50	0.44	0.76	1.32	0.47	0.76	3.05	3.96	33	67
	300	0.41	0.35	0.75	1.34	0.48	0.75	2.48	2.78	37	63
3c	79	0.52	0.49	0.68	1.18	0.43	0.69	4.24	4.38	38	62
	300	0.41	0.37	0.70	1.18	0.45	0.71	2.86	3.13	41	59

* δ is the isomer shift, Δ is the quadrupole splitting, Γ_{exp} is the line width, *I* is the line intensity, and *S* is the relative area of a subspectrum.

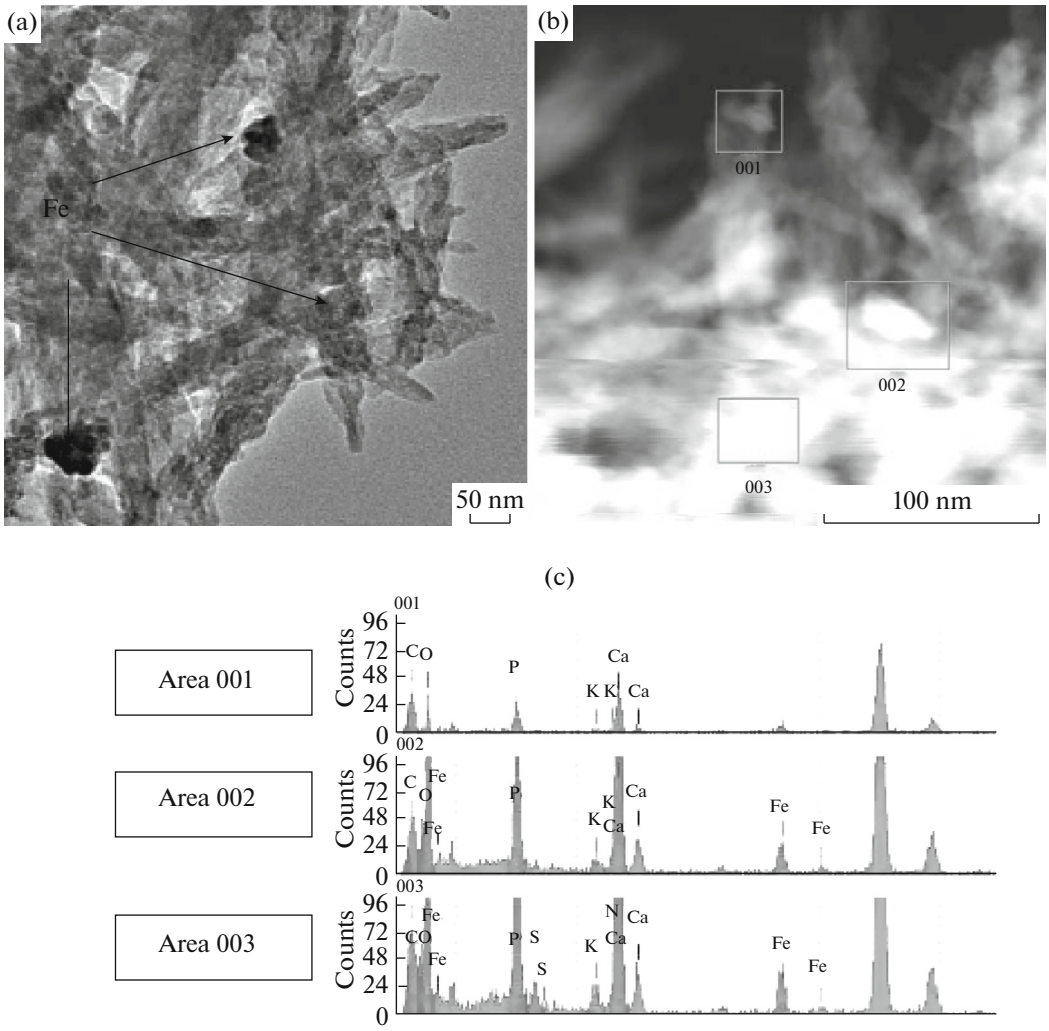

Fig. 5. (a) TEM image of iron-containing nanoparticles in sample **3a** and (c) energy-dispersive electron probe analysis data for the areas shown in the STEM image (b).

The doublet with the smaller quadrupole splitting value (Table 2, subspectrum 1) has a smaller line width (and smaller area) and corresponds to iron atoms in a more symmetric and ordered environment, for example, in the bulk of a nanosized particle. The doublet with the larger area, larger quadrupole splitting value, and larger line width (Table 2, subspectrum 2) corresponds to iron atoms in a less symmetric environment and disordered part of the sample, for example, on the surface of nanosized particles [31].

The isomer shifts for the doublets of samples **1x** at various temperatures noticeably differ from the other samples and are consistent with the data for iron(III) oxo hydroxo compounds in alkaline media [32]. For the samples obtained after the introduction of iron at the second and third stages (**2c** and **3c**), the isomer shifts, especially for the inner doublet, are noticeably larger (Table 2). This can be evidence that the major iron-containing phase in these samples is that of iron phosphate compounds, since they are characterized by higher isomer shifts [33, 34].

In addition, the **Nc** samples exhibit essentially larger quadrupole splittings and line widths of each subspectrum (Table 2). For the **Na** samples, the areas of the "amorphous" part (subspectrum 2) change within 70–80%, whereas for the samples annealed at 500°C, the fraction of the corresponding subspectrum decreases to 60–70% (Table 2). These facts are evidence that annealing leads to a change in both the surface-to-bulk ratio of iron atoms and their environment. The latter becomes less symmetric and less homogeneous; i.e., when annealed, the iron-containing phase undergoes the incomplete thermal transformation [35].

Thus, the formation of aqueous suspensions of nano-HAP in the presence of iron(III) sulfate has been studied. It has been demonstrated that parameters of the reaction products, such as particle size,

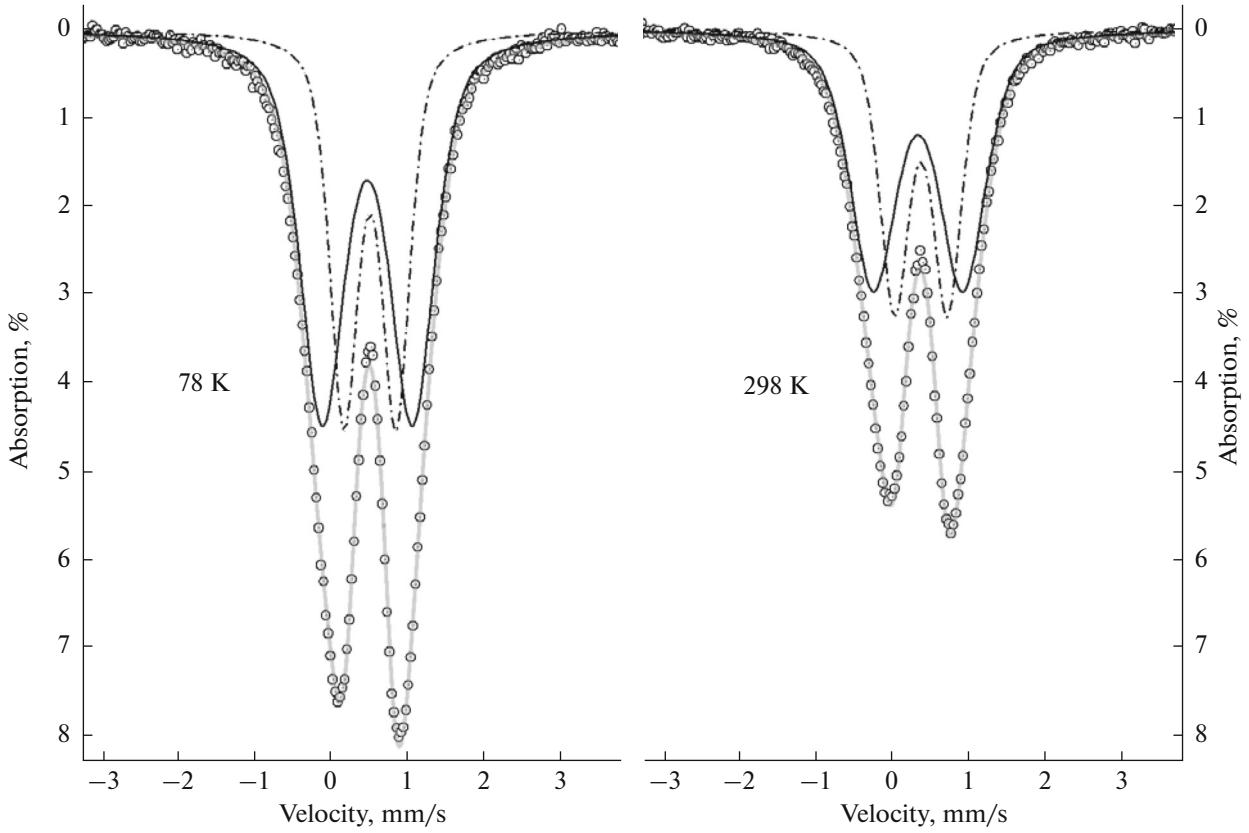

Fig. 6. Mössbauer spectra of sample **3c** at different temperatures and their description models.

morphology, and phase composition, can be modified by varying the moment of introduction of the modifying compound into the reactor. The strongest effect is achieved when the iron-containing solution is introduced before the onset of the basic synthesis reaction. In this case, the impurity particle of calcium sulfate and iron(III) hydroxide can act as HAP aggregation and growth centers. In addition, the ability of iron(III) ions to suppress the HAP crystallization is most pronounced (formation of the amorphized HAP phase). The introduction of an iron-containing solution at later stages has an effect (insignificant) mainly on the HAP particle size. The data obtained in this study demonstrate that iron itself can form both its own nanophase (oxo hydroxo species in samples **1a** and phosphate species in samples **2a** and **3a**) and ion clusters adsorbed on the HAP nanoparticle surface. Being annealed at 500°C, the iron-containing particles undergo the incomplete thermal transformation. The relative content of different iron species in samples can be tailored by varying both the moment of introduction of the modifying agent and its concentration. The strategy of introduction of bioactive metal ions at early stages of HAP synthesis can be used for producing bone tissue precursors with different morphology and microcomponent content. If it is necessary to use HAP as the carrier of magnetic particles, iron ions should be introduced at final stages of HAP synthesis in relatively large amounts. However, under our experimental conditions, it is inadvisable to use iron sulfate for increasing the iron content in samples because of the formation of large amounts of calcium sulfate as a byproduct.

ACKNOWLEDGMENTS

We are grateful to the research and educational shared facility center "Nanochemistry and Nanomaterials" at the Moscow State University for help in studying the morphology of the samples.

REFERENCES

1. S. M. Barinov and V. S. Komlev, *Bioceramics Based on Calcium Phosphates* (Nauka, Moscow, 2005), p. 10 [in Russian].
2. M. Bohner, Injury **31**, D37 (2000).
3. M. Vallet-Regi, J. Chem. Soc., Dalton Trans., 97 (2001).
4. D. C. Carvalho, L. G. Pinheiro, A. Campos, et al., Appl. Catal., A: Gen. **471**, 39 (2014).
5. Zhenping Qu, Yahui Sun, Dan Chen, and Yi Wang, J. Mol. Catal. A: Chem. **393**, 182 (2014).

6. M. Pogosova, D. Provotorov, A. Eliseev, et al., Dyes Pigments **113**, 96 (2015).
7. G. Salviulo, M. Bettinelli, U. Russo, et al., J. Mater. Sci. **46**, 910 (2011).
8. Chun-Han Hou, Sheng-Mou Hou, Yu-Sheng Hsueh, et al. Biomaterials **30**, 3956 (2009).
9. A. Tampieri, T. D'Alessandro, M. Sandri, et al., Acta Biomater. **8**, 843 (2012).
10. Kunfeng Zhao, Botao Qiao, Junhu Wang, et al., Chem. Commun. **47**, 1779 (2012).
11. H. R. Low, N. Phonthammachai, A. Maignan, et al., Inorg. Chem. **47**, 11774 (2008).
12. I. Mayer, H. Diab, and I. Felner, J. Inorg. Biochem., 129 (1992).
13. I. V. Melikhov, V. F. Komarov, A. V. Severin, et al., Dokl. Phys. Chem. **373**, 355 (2000).
14. P. W. Brown, J. Am. Ceram. Soc. **75**, 17 (1992).
15. *Unified Water Analysis Methods*, Ed. by Yu. Yu. Lur'e (Khimiya, Moscow, 1973) [in Russian].
16. S. S. Gorelik, Yu. A. Skakov, and L. N. Rastorguev, *X-ray Powder and Electron-Optical Analysis* (MISIS, Moscow, 2002) [in Russian].
17. N. C. Collier, N. B. Milestone, J. Hill, et al., Waste Manage. 26 (2006).
18. S. Scaccia, M. Carewska, A. D. Bartolomeo, et al., Thermochim. Acta **383**, 145 (2002).
19. J. O. Nriagu, Geochim. Cosmochim. Acta **36**, 459 (1972).
20. B. M. Al-Hasni, G. Mountjoy, and E. Barney, J. Non-Cryst. Solids **380**, 141 (2013).
21. A. S. Posner, N. C. Blumenthal, and F. Betts, in *Phosphate Minerals,* Ed. by G. O. Nriagu and P. B. Moore (Springer, Berlin, 1984).
22. J. M. Hughes, M. Cameron, and K. D. Crowley, Am. Mineral. **74**, 870 (1989).
23. ASTM-41-224, 41-225.
24. J. Herrero, O. Artieda, and W. H. Hudnall, Soil Sci. Soc. Am. J. **73**, 1757 (2009).
25. N. Prieto-Taboada, O. Gómez-Laserna, I. Martínez-Arkarazo, et al., Anal. Chem. **86**, 10131 (2014).
26. H. Weiss and M. F. Bräu, Angew. Chem., Int. Ed. Engl. **48**, 3520 (2009).
27. A. Y. Polyakov, A. E. Goldt, T. A. Sorkina, et al., Cryst. Eng. Commun. **14**, 8097 (2012).
28. C. Díaz-Aguila, M. Morales, E. Baggio-Saitovitch, et al., III Congreso Internacional de Biomateriales BIOMAT'03, 2003.
29. E. I. Suvorova, V. V. Klechkovskaya, V. F. Komarov, et al., Crystallogr. Rep. **51**, 881.
30. D. A. Pankratov, Inorg. Mater. **50**, 82 (2014).
31. D. A. Pankratov, A. A. Veligzhanin and Y. V. Zubavichus, *Russ. J. Inorg. Chem*. **58**, 67 (2013).
32. D. A. Pankratov and Y. M. Kiselev, Russ. J. Inorg. Chem. **54**, 1451 (2009).
33. M. D. Dyar, E. R. Jawin, E. Breves, et al., Am. Mineral. **99**, 914 (2014).
34. J. Mingzhi, C. Xianhao, X. Weiming, et al., Hyperfine Interact. **41**, 645 (1988).
35. M. M. Gadgil and S. K. Kulshreshtha, J. Solid State Chem. **111**, 357 (1994).

Translated by G. Kirakosyan